IOP PUBLISHING JOURNAL OF PHYSICS D: APPLIED PHYSICS

J. Phys. D: Appl. Phys. **41** (2008) 185304 (10pp) doi:10.1088/0022-3727/41/18/185304

Investigation of aluminium and indium *in situ* doping of chemical bath deposited CdS thin films

Hani Khallaf[1], Guangyu Chai[2], Oleg Lupan[1,3], Lee Chow[1,4], S Park[1] and Alfons Schulte[1]

[1] Department of Physics, University of Central Florida, Orlando, FL 32816, USA
[2] Apollo Technologies, Inc., 205 Waymont Court, Suite 111, Lake Mary, FL 32746, USA
[3] Department of Microelectronics and Semiconductor Devices, Technical University of Moldova, 168 Stefan cel Mare Boulevard, MD-2004 Chisinau, Republic of Moldova

E-mail: chow@mail.ucf.edu

Received 30 June 2008, in final form 23 July 2008
Published 29 August 2008
Online at stacks.iop.org/JPhysD/41/185304

Abstract

Aluminum and indium *in situ* doping of CdS using chemical bath deposition (CBD) is investigated. The effects of Al and In-doping on optical properties as well as on electrical properties, crystal structure, chemistry and morphology of CdS films are studied. Al doping of CdS using CBD is shown to be successful where a resistivity as low as $4.6 \times 10^{-2}\ \Omega$ cm and a carrier density as high as 1.1×10^{19} cm^{-3} were achieved. The bandgap of Al-doped films decreases to a minimum of 2.26 eV, then slightly increases and finally saturates at 2.30 eV as the [Al]/[Cd] ratio in solution increases from 0.018 to 0.18. X-ray diffraction studies showed Al^{3+} ions entering the lattice substitutionally at low concentration and interstitially at high concentration. Phase transition, due to annealing, and induced lattice damage, due to doping, were detected by micro-Raman spectroscopy. Film stoichiometry was found to be sensitive to Al concentration, while film morphology was unaffected by Al doping. Indium doping using CBD, however, was found to be highly unlikely due to the low solubility of indium sulfide. Instead, the formation of InS/In_2S_3 dominated the deposition process over CdS.

(Some figures in this article are in colour only in the electronic version)

1. Introduction

Chemical bath deposition (CBD) is known to be a simple, low temperature and inexpensive large-area deposition technique for group II–VI semiconductors such as CdS. It has been used in CdS thin films deposition since the 1960s [1, 2]. CdS films grown by CBD are known to be highly stoichiometric and exhibit a high dark resistance. A summary of dark resistances reported in the literature for several CBD-CdS thin films is shown in table 1. We have shown earlier [3] that with NH_3 as the complexing agent and thiourea as the sulfur source, using different Cd sources affects the stoichiometry as well as dark resistivity of CBD-CdS films. A direct relationship between sulfur deficiency and carrier concentration (CC)/resistivity in CdS films was established. It was shown that using $CdCl_2/CdI_2$ as Cd sources results in highly stoichiometric films with an S : Cd ratio of 1.00 : 1.00, while using $Cd(CH_3COO)_2$ and $CdSO_4$ decreased that ratio to 1.00 : 1.06 and 1.00 : 1.09, respectively. Consequently, the dark resistivity of $Cd(CH_3COO)_2$ and $CdSO_4$-based CdS films was, respectively, 10 and 50 times smaller than that of $CdCl_2/CdI_2$-based CdS films. Yet, to be useful in solar cells as well as other optoelectronic applications, dark resistivity of CBD-CdS needs to be further reduced. In another work [4], we have shown that using nitrilotriacetic acid and N_2H_4 together as a complexing agent instead of NH_3 results in a S : Cd ratio of 1.00 : 1.08 instead of 1.00 : 1.00 for $CdCl_2$-based films, but this was at the expense of the growth rate as well as film quality due to domination of the homogenous reaction over the heterogeneous reaction in the deposition process.

One approach to reduce the dark resistivity of CBD-CdS is *in situ* doping. Over the past two decades, *in situ* doping of

[4] Author to whom any correspondence should be addressed.

Table 1. A summary of the dark resistivity of some CBD-CdS films reported in the literature and the corresponding Cd source used.

	Cd source	Other reagents used in solution	$T_{deposition}$ (°C)	ρ_{dark} (Ω cm)	References
1.	$CdCl_2$	NH_4OH /NH_4Cl/TU[b]	80	10^{6-7}	[7]
	$CdAc_2$[a]			10^{6-7}	
2.	$CdCl_2$	NH_4OH/NH_4Cl/TU	>40	10^{6-8}	[9]
	CdI_2	NH_4OH/NH_4I/TU	>60	10^{8-10}	
3.	$CdSO_4$	NH_4OH/TU	60–85	10^7	[5]
4.	$CdSO_4$	NH_4OH/N_2H_4/TU	60	10^{10}	[6]
5.	$CdSO_4$	NH_4OH/TU	70	10^8	[10]
6.	$CdCl_2$	NH_4OH/NH_4Cl/TU	70	10^3	[3]
	CdI_2	NH_4OH/NH_4I/TU		10^3	
	$CdAc_2$	NH_4OH/NH_4Ac/TU		10^2	
	$CdSO_4$	NH_4OH/$(NH_4)_2SO_4$/TU		10^1	
7.	$CdAc_2$	NH_4OH/NH_4Ac/TU	50–90	10^{4-6}	[11]
8.	$CdAc_2$	TEA + NH_4OH/TU	30–85	10^9	[12]
9.	$CdAc_2$	$Na_3C_6H_5O_7$/NH_4OH/TU	50–90	10^8	[13]
10.	$Cd(NO_3)_2$	NH_4NO_3/NaOH/TU	20	$>10^{12}$	[8]

[a] Ac = Acetate; $(CH_3COO)^-$.
[b] TU = Thiourea; $SC(NH_2)_2$.

CBD-CdS using Cu [14, 15], Li [16, 17], Na [18], Al [19, 20] and B [11, 21] has been reported. Ag doping of CBD-CdS was carried out using the ion exchange process [22, 23] and In-doped CdS films were grown by co-evaporation of CdS and indium [24, 25]. In this work, *in situ* doping of CBD-CdS using group III elements, namely, Al and In, is investigated. The objective of this work is to investigate the effectiveness of Al^{3+}/In^{3+} doping through CBD. Transmittance and reflectance measurements of doped films were carried out to study the effect of Al/In doping on the optical properties and bandgap of CdS films. The resistivity, CC and mobility of doped films were acquired using Hall effect measurements. The crystal structure and crystal quality and phase transition were determined using x-ray diffraction (XRD) and micro-Raman spectroscopy. Film morphology was studied using scanning electron microscopy (SEM). Film chemistry and binding states were studied using x-ray photoelectron spectroscopy (XPS).

2. Experimental details

CdS films were prepared using stock solutions of $CdSO_4$ (0.038 M), $(NH_4)_2SO_4$ (0.076 M), NH_3OH (29.4%) and $(NH_2)_2CS$ (0.076 M). Films were grown on 38 mm × 38 mm × 1 mm glass substrates (Schott Borofloat glass, supplied by S.I. Howard Glass Co., Inc.). Al/In doping was carried out by adding the appropriate amount from a 4 mM stock solution of $Al_2(SO_4)_3$/$InCl_3$ to the main solution. The deposition temperature was kept constant at 85 °C. Details of the growth process have been previously reported [3]. Prior to the deposition of CdS films, glass substrates were cleaned by Liqui-Nox soap (supplied by Alconox, Inc.), then washed in de-ionized water, rinsed in acetone/methanol, washed again in de-ionized water, etched with dilute HCl for 2–3 min, etched with $H_2O_2 : H_2SO_4$ (1 : 1 solution) for 5 min, etched in dilute HF for 1 min and then cleaned ultrasonically in de-ionized water for 5 min. After deposition, all films were annealed at 300 °C in argon ambient for 1 h.

An Alpha-step 500 surface profilometer (Tencor) was used to determine the film thickness. Specular transmittance measurements were carried out at room temperature with unpolarized light at normal incidence in the wavelength range from 350 to 1200 nm using a Cary 500 (Varian) double beam UV/VIS spectrophotometer. Specular reflectance measurements have been carrier out at an angle of incidence of 7° in the same wavelength range. The optical absorption coefficient α was calculated for each film using the equation [26]

$$T = (1 - R)^2 \exp(-\alpha t), \tag{1}$$

where T is the transmittance, R is the reflectance and t is the film thickness.

The absorption coefficient α is related to the incident photon energy $h\nu$ as

$$\alpha = \frac{K(h\nu - E_g)^{n/2}}{h\nu}, \tag{2}$$

where K is a constant, E_g is the optical bandgap and n is equal to 1 for a direct bandgap material such as CdS. The bandgap was determined for each film by plotting $(\alpha h\nu)^2$ versus $h\nu$ and then extrapolating the straight line portion to the energy axis. XRD was carried out using Rigaku D XRD unit (with 40 kV, 30 mA CuKα radiation, $\lambda = 0.154\,06$ nm). The sample was mounted at 2.5° and scanned from 25° to 55° in steps of 0.02° with a scan rate of 1.2° min^{-1}. Resistivity, mobility and carrier density were evaluated by Hall measurements at room temperature in a Van der Pauw four-point probe configuration, using indium contacts, in an automated Hall effect system (Ecopia HMS-3000, Bridge Technology, Chandler Heights AZ, USA) with a 0.55 T magnetic induction. Micro-Raman scattering was performed at room temperature with a Horiba Jobin Yvon LabRam IR system at a spatial resolution of 2 μm in a backscattering configuration. A 632.8 nm line of a helium–neon laser was used for off-resonance excitation with less than 4 mW power at the sample. The spectral resolution

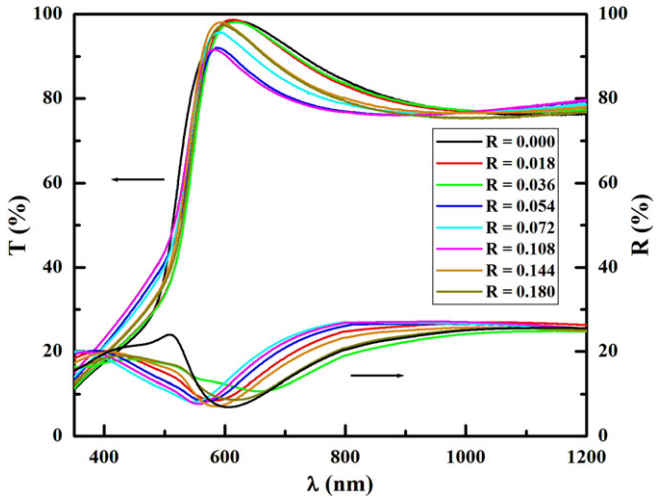

Figure 1. Specular transmittance and reflectance spectra of Al-doped CdS films grown at different [Al]/[Cd] ratios (R denotes the [Al]/[Cd] ratio and $R = 0.000$ refers to the undoped film).

was 2 cm^{-1}, and the instrument was calibrated to the same accuracy using a naphthalene standard. XPS was performed on a Physical Electronics PHI 5400 ESCA using monochromatic Mg Kα radiation at 1253.6 eV. Each of the XPS spectra was acquired from 30 repeated sweeps. Spectra were corrected from charging effects by referencing the adventitious C 1s peak to 284.6 eV. SEM micrographs were obtained using JEOL 6400F SEM at an acceleration voltage of 10 kV.

3. Results and discussion

3.1. Investigation of aluminum doping

Figure 1 shows optical transmittance and reflectance spectra of all Al-doped films grown at different [Al]/[Cd] ratios. The [Al]/[Cd] ratio in solution was varied from 0.018 to 0.18. It should be noted that a ratio of zero was assigned to the undoped film (purely CdS). All films exhibit a high transmittance that exceeds 80% in the visible region of the spectrum and exceeds 90% right before the absorption edge. The variation in transmittance with the [Al]/[Cd] ratio is likely attributed to variation in the film thickness. Table 2 shows that the thickness of doped films increases at first and then decreases. This may explain why the transmittance drops at first and then rises as the [Al]/[Cd] ratio increases. A red shift in the absorption edge towards a lower band gap is noticed in almost all doped films. The magnitude of the red shift was found to fluctuate as the [Al]/[Cd] ratio increases. Using transmittance and reflectance data, the absorption coefficient α was calculated (using equation (1)) and was then used to determine the band gap, as shown in figure 2. As shown in figure 3, the bandgap of the doped films decreases to a minimum of 2.26 eV at a ratio of 0.018 and 0.036, then slightly increases and finally saturates at 2.30 eV as the [Al]/[Cd] ratio exceeds 0.10. The undoped film has a band gap of 2.41 eV which agrees well with the 2.42 eV band gap of single crystal CdS [27].

XRD patterns of Al-doped films as well as undoped film are shown in figure 4. We have shown earlier [3] that as-grown

Table 2. Film thickness of Al-doped CdS films grown at different [Al]/[Cd] ratios (the 0.000 ratio is assigned to the undoped film).

[Al]/[Cd] ratio	Film thickness (Å)
0.000	1100
0.018	1300
0.036	1500
0.054	1500
0.072	1200
0.108	1100
0.144	1000
0.180	1000

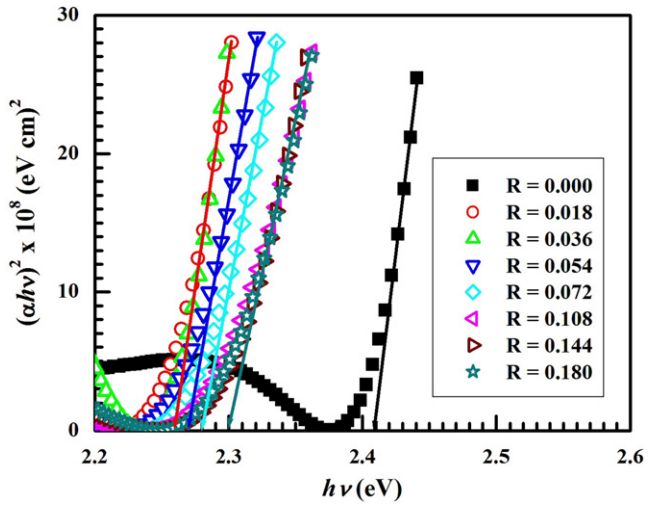

Figure 2. Optical bandgap calculations of Al-doped CdS films grown at different [Al]/[Cd] ratios (R denotes the [Al]/[Cd] ratio and $R = 0.000$ refers to the undoped film).

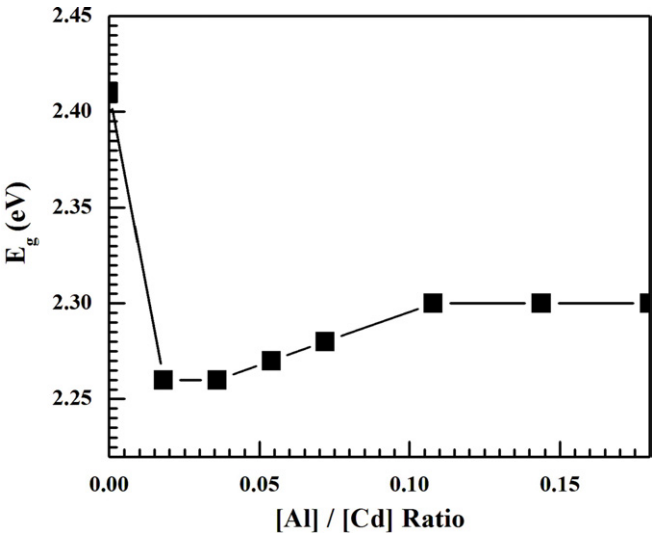

Figure 3. Optical bandgap of Al-doped CdS films as a function of the [Al]/[Cd] ratio.

CdS films are polycrystalline and cubic in nature, with a preferred orientation along the (1 1 1) direction. We have also shown that the degree of texture along the (1 1 1) orientation highly depends on the Cd source used. When $CdSO_4$ is being used as the Cd source, which is the case in this work, the (2 2 0) and (3 1 1) peaks are almost totally suppressed and only

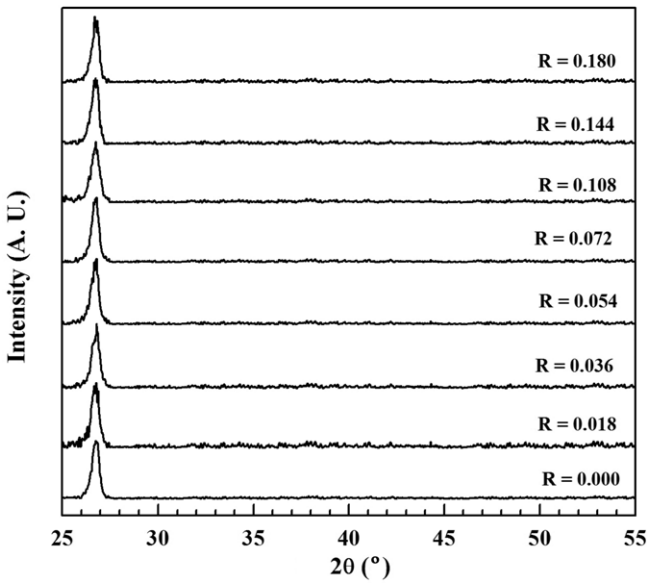

Figure 4. XRD pattern of Al-doped CdS films grown at different [Al]/[Cd] ratios (R denotes the [Al]/[Cd] ratio and $R = 0.000$ refers to the undoped film).

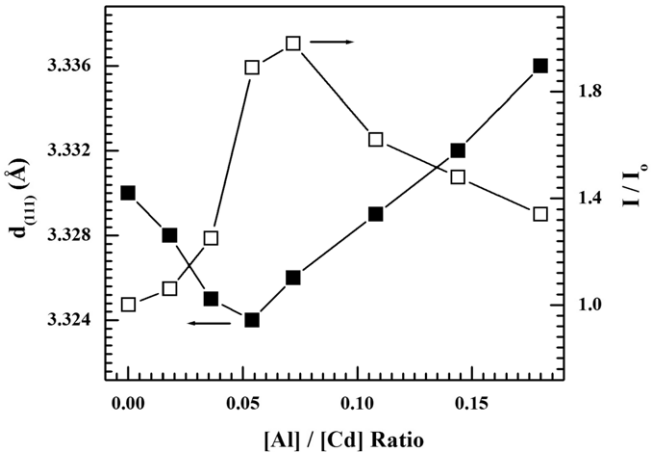

Figure 5. Average (1 1 1) interplanar distance $d_{(1\,1\,1)}$ and relative intensity I/I_o of the (1 1 1) peak with respect to that of the undoped film as a function of the [Al]/[Cd] ratio.

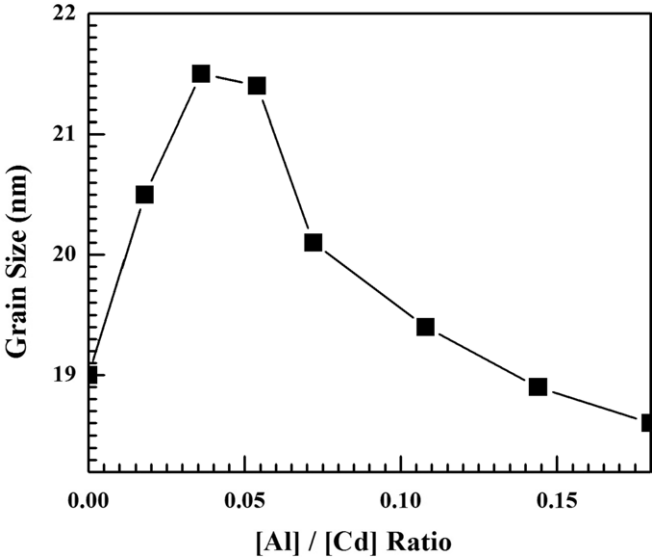

Figure 6. Grain size dependence on the [Al]/[Cd] ratio.

the (1 1 1) peak is detected. Now, keeping in mind that, at room temperature, cubic CdS is considered a metastable phase while hexagonal CdS is the stable phase, thermal annealing may cause a phase transition from the cubic phase to the hexagonal phase. The critical point for such a phase transition was reported to be 300 °C [28], above which the hexagonal phase predominates over the cubic phase. Since all films were annealed at 300 °C, it is difficult to determine if the peak shown in figure 4 is the (1 1 1) peak of the cubic phase or the (0 0 2) peak of the hexagonal phase which coincides with the (1 1 1) peak. We will show later in this work that there is some phase transition that has been detected by micro-Raman spectroscopy. In order to avoid confusion, we will refer to the peak detected as the (1 1 1) peak of cubic CdS. As shown in figure 4, no peaks of Al, AlS or Al_2S_3 were detected, which indicates that incorporation of Al^{3+} ions does not change the crystal structure of the CdS film. The average (1 1 1) interplanar distance $d_{(1\,1\,1)}$ was calculated using the formula $\lambda = 2d \sin\theta$, where λ is the x-ray wavelength (1.5406 Å) and θ is the Bragg angle. As shown in figure 5, as the [Al]/[Cd] ratio increases, the spacing of the (1 1 1) lattice planes decreases below that of the undoped film until it reaches a minimum at a ratio of 0.055 and then it starts to increase as the [Al]/[Cd] ratio increases, and once that ratio exceeds 0.11, the $d_{(1\,1\,1)}$ value goes beyond that of the undoped CdS film. Now, since the ionic radius of Al^{3+} (0.50 Å) is smaller than that of Cd^{2+} (0.97 Å) [29], this suggests that at a low [Al]/[Cd] ratio, Al^{3+} ions replace Cd^{2+} ions in the lattice substitutionally which in turn results in a smaller $d_{(1\,1\,1)}$ value than that of the undoped CdS film. As this ratio increases beyond 0.055, Al^{3+} ions start to enter the lattice both substitutionally and interstitially which caused the $d_{(1\,1\,1)}$ values to increase again. As the [Al]/[Cd] ratio exceeds 0.11, most Al^{3+} ions incorporated in the lattice are in interstitial sites which caused $d_{(1\,1\,1)}$ values to exceed that of the undoped film. This will have an impact on the electrical properties of Al-doped films as Hall measurements will show later.

Figure 5 also shows the relative intensity of the (1 1 1) peak with respect to that of undoped film. As shown, all doped films have a relative intensity higher than one. It is worth noting that the way the relative intensity behaves as a function of the [Al]/[Cd] ratio is almost opposite to that of the $d_{(1\,1\,1)}$ values. This confirms our conclusion that Al^{3+} ions enter the lattice substitutionally at low concentration and interstitially at high concentration. The grain size shown in figure 6 was calculated using the formula $D = 0.9\lambda/\beta \cos\theta$, where β is the full width at half maximum (FWHM) in radians. In agreement with the thickness measurements in table 2, the grain size increases with the [Al]/[Cd] ratio, and then as this ratio exceeds 0.055, the grain size decreases as the [Al]/[Cd] ratio increases.

This can also explain the way the bandgap varies with the [Al]/[Cd] ratio. As suggested by Lokhande and Pawar [19] and later by Akintunde [20], incorporation of Al as well as sulfur deficiency in Al-doped films gives rise to donor levels

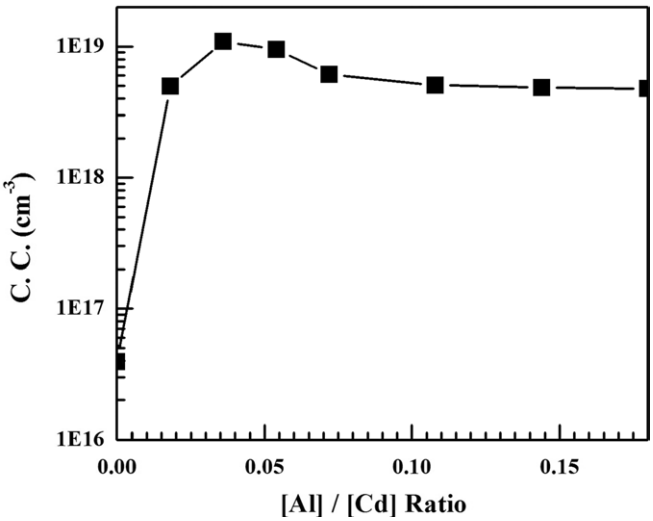

Figure 7. CC dependence on the [Al]/[Cd] ratio.

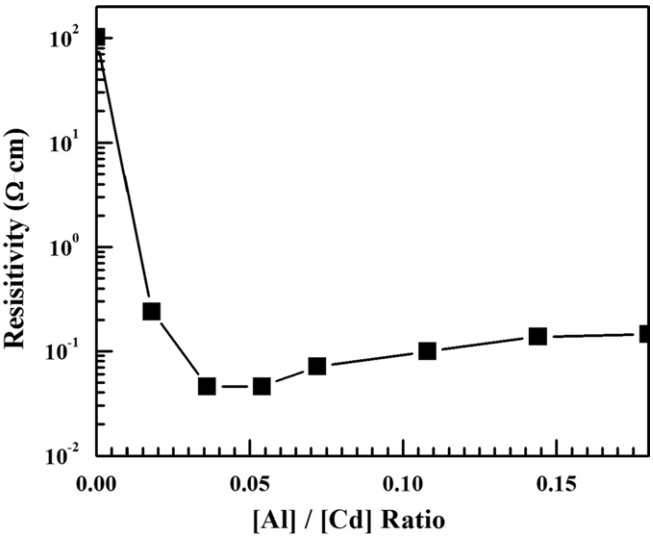

Figure 8. Dark resistivity as a function of the [Al]/[Cd] ratio.

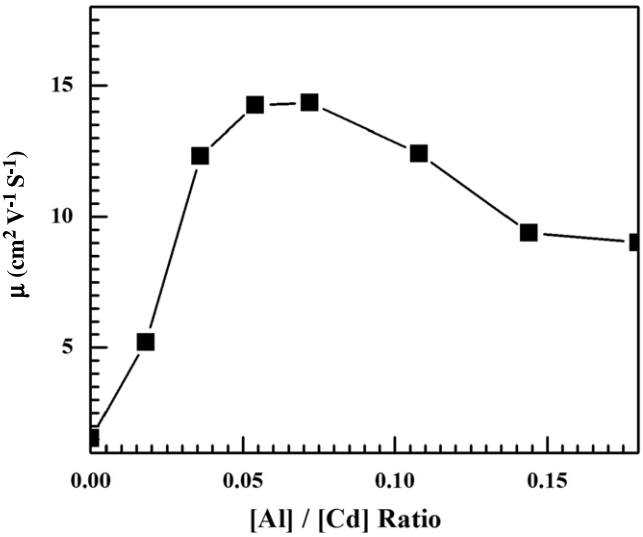

Figure 9. Variation of Hall mobility with the [Al]/[Cd] ratio.

in the bandgap of CdS. As the Al concentration increases which in turn increases the sulfur deficiency, the donor levels become degenerate and merge in the conduction band of CdS, causing the conduction band to extend into the bandgap which reduces the band gap. The reason the bandgap increases as the [Al]/[Cd] ratio goes beyond 0.055 may be attributed to the decrease in the grain size of the doped films (figure 6) which causes an increase in the lattice strain in the film. We have observed in a previous work [4] that such an increase in the lattice strain (due to decrease in the film thickness/grain size) increases the bandgap of CdS films.

Figure 7 shows the CC as a function of the [Al]/[Cd] ratio. The undoped film has a CC of about 4×10^{16} cm^{-3}. The CC increases with the [Al]/[Cd] ratio until it reaches a maximum ($\sim 1.1 \times 10^{19}$ cm^{-3}) at a ratio of 0.036, and then decreases as the ratio exceeds 0.055 until it drops to 4.7×10^{18} cm^{-3} at a ratio of 0.18. The film resistivity as a function of the [Al]/[Cd] ratio is shown in figure 8. The dark resistivity drops from 1.03×10^2 Ω cm (undoped film) to a minimum of 4.6×10^{-2} Ω cm at a ratio of 0.036 and 0.055, after which it increases until it reaches 1.45×10^{-1} Ω cm at a ratio of 0.18. This agrees with the $d_{(1\,1\,1)}$ value variation with the [Al]/[Cd] ratio. As we pointed out earlier, at low [Al]/[Cd] ratios, Al^{3+} ions replace the Cd^{2+} ions in the lattice substitutionally, which increases the CC of the doped films and decreases the resistivity. However, at higher ratios, Al^{3+} ions start to enter the lattice both substitutionally and interstitially. Interstitial Al^{3+} ions will act as recombination centres decreasing the CC and increasing the resistivity. Such behaviour of CC as well as dark resistivity has been also reported by Lokhande and Pawar [19] and by Akintunde [20].

It should be noted that, although CC at the 0.055 ratio (9.52×10^{18} cm^{-3}) is less than that at the 0.036 ratio ($\sim 1.1 \times 10^{19}$ cm^{-3}), both films appear to have the same resistivity. This can be understood by considering the Hall mobility (μ) values shown in figure 9. The Hall mobility at a ratio of 0.055 was 14.25 (cm^2 V^{-1} S^{-1}) while the Hall mobility at a ratio of 0.036 was 12.33 (cm^2 V^{-1} S^{-1}). This difference compensated for the CC difference and resulted in a similar resistivity value. In general, the Hall mobility values observed agree with what was reported earlier by Bertrán *et al* [24] and Hayashi *et al* [25]. Variation of μ with respect to the [Al]/[Cd] ratio agrees to some extent with the way grain size changes with respect to the [Al]/[Cd] ratio (figure 6).

Figure 10 shows micro-Raman spectra for all Al-doped films. All films show the same CdS characteristic peak at about 303 cm^{-1}. Another CdS characteristic peak, 2 longitudinal optical (LO) [38], is barely noticeable at about 600 cm^{-1}. A closer look at the main peak at 303 cm^{-1} shows the peak being asymmetric, suggesting a superposition of more than one mode. Figure 11 shows the deconvolution of the 303 cm^{-1} peak of the film grown at the [Al]/[Cd] ratio of 0.018, using the Gaussian fit from which the peak position and FWHM have been obtained. It should be noted that the Gaussian fit gave a better fit than the Lorentzian fit, which may be due to film defects and induced lattice damage because of Al doping, as will be discussed later. As shown in figure 11, that peak

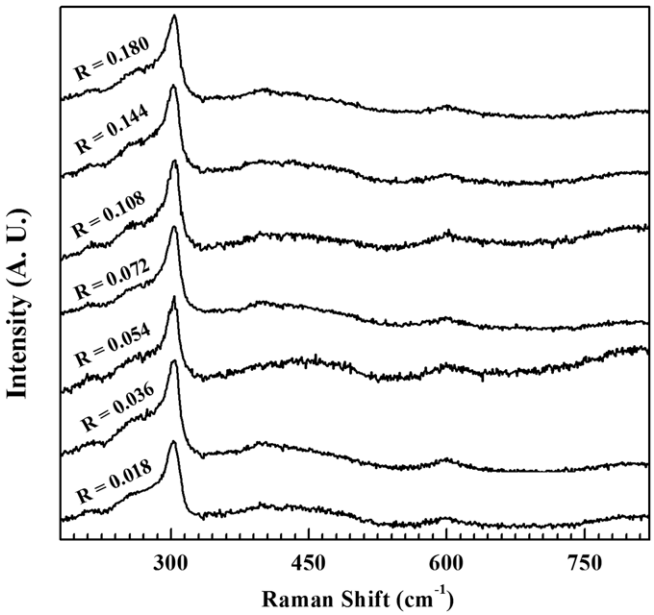

Figure 10. Raman spectra of Al-doped films grown at different [Al]/[Cd] ratios (*R* denotes the [Al]/[Cd] ratio).

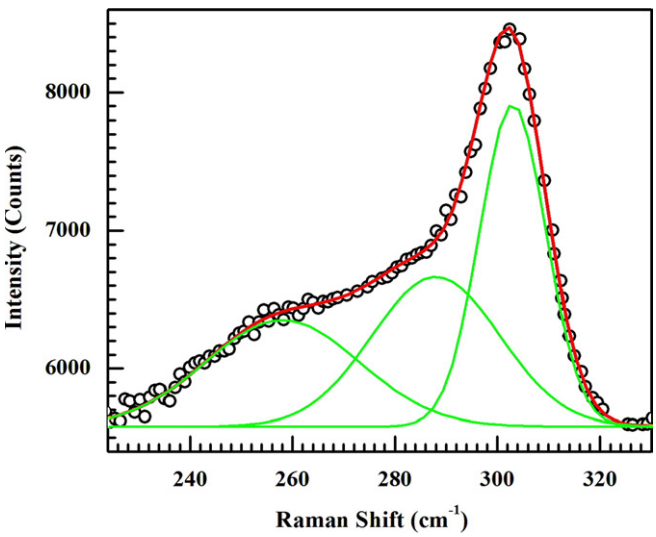

Figure 11. Deconvolution of the 303 cm^{-1} Raman peak of the film grown at the [Al]/[Cd] ratio of 0.018 into three peaks using the Gaussian fit.

can be deconvoluted into three different peaks: the highest at 302.8 cm^{-1} with an FWHM of 12.8 cm^{-1}, the middle at 287.5 cm^{-1} with an FWHM of 25.0 cm^{-1} and the lowest peak at 258.3 cm^{-1} with an FWHM of 30.0 cm^{-1}. The prominent peak at 302.8 cm^{-1} is attributed to either the cubic 1LO phonon [36] or the hexagonal A_1(LO)/E_1(LO) phonons [32]. The peak observed at 258.3 cm^{-1} is the E_2 peak of hexagonal CdS [33, 35]. However, the peak observed at 287.5 cm^{-1} is attributed to a shift in either the transverse optical (TO) peak of cubic CdS [36] or the E_1(TO) peak of hexagonal CdS [35]. This Raman shift results from a phase transition in the CdS film, from cubic to hexagonal, due to annealing at 300 °C. Zelaya-Angel *et al* [30] reported a similar shift for CdS films annealed at 350 °C, where they observed the E_1(TO) phonon at 276 cm^{-1} instead of 240 cm^{-1}. According to their calculations, the Raman shift, due to phase transition in CdS, should be about 18% which causes the E_1(TO) peak to shift from 240 cm^{-1} (original position in hexagonal CdS [35]) to 283 cm^{-1}. A similar shift in the TO peak of cubic CdS (originally at 246 cm^{-1} [36]) will position this peak at about 290 cm^{-1}. Since the peak they observed for the annealed CdS film was at 276 cm^{-1}, they ruled out the TO phonon possibility and attributed this peak to a shift in the E_1(TO) peak of hexagonal CdS. In our work, however, this peak is observed at 287.5 cm^{-1} rather than at 276 cm^{-1}, which may be attributed to the TO phonon of cubic CdS rather than the E_1(TO) peak of hexagonal CdS. No peaks were detected for the A_1(TO) phonon of hexagonal CdS. Table 3 lists some of the experimental and theoretical values reported for A_1(LO), A_1(TO), E_1(LO), E_1(TO) and E_2 phonons for hexagonal single crystal CdS as well as values of 1LO, 2LO, and TO phonons for cubic CdS.

Figure 12 shows an example of the effect of annealing on micro-Raman spectra of the CdS undoped film. As shown in figure 12(*b*), the 1LO peak observed at 303 cm^{-1} for the as-grown undoped film is clearly symmetric. A Gaussian fit is shown in the inset of figure 12(*b*), according to which the peak has an FWHM of ∼16.6 cm^{-1}. Figure 12(*c*) shows micro-Raman for the same undoped film after annealing; the peak is obviously asymmetric. Deconvolution of the peak using the Gaussian fit is shown in the inset of figure 12(*c*). It consists of three different peaks at 258.5, 288 and 302.5 cm^{-1}. This proves that the asymmetry in the main peak at ∼303 cm^{-1} is due to annealing, not Al doping. It was noticed that the FWHM of the peak at 302.5 cm^{-1} of the annealed film is 12.2 cm^{-1}, which is much smaller than that of the as-grown film (16.6 cm^{-1}). This indicates an enhancement in film crystallinity due to annealing. The FWHM of the 1LO phonon of single crystal CdS was reported to be in the range 9–10 cm^{-1} [31]. It is worth noting that the hump observed between 400 and 500 cm^{-1} is due to fluorescence from the substrate, as shown in figure 12(*a*).

A similar deconvolution of the 303 cm^{-1} peak was carried out for all Al-doped films. Figure 13 shows the position and FWHM of the E_2, TO and cubic 1LO or hexagonal A_1(LO)/E_1(LO) peaks calculated from the Gaussian fit. Apparently, the position and FWHM of both E_2 and TO peaks are on average constant regardless of the [Al]/[Cd] ratio used. The average position of the E_2 peak was found to be 258.3 cm^{-1} (figure 13(*a*)) which agrees well with the 256 cm^{-1} [33] and the 257 cm^{-1} [35] values of E_2 that have been reported earlier (table 3). The average position of the middle peak (figure 13(*b*)) is 288 cm^{-1} which confirms our conclusion that this peak is attributed to a shift in the TO peak of cubic CdS. However, as shown in figure 13(*c*), the position and FWHM of the cubic 1LO or the hexagonal A_1(LO)/E_1(LO) peak are sensitive to the [Al]/[Cd] ratio. As that ratio increases, the peak position and FWHM increase. The increase in FWHM is, however, more significant which implies an increase in the induced lattice damage as the [Al]/[Cd] ratio increases.

Figure 14 shows XPS multiplex spectra for the undoped film and the Al-doped films grown at [Al]/[Cd] ratios of 0.036 and 0.18. In all three cases, the binding energy of the S 2p peak (figure 14(*a*)) is 161.7 eV which is in the range characteristic of

Table 3. A summary of E_1 (LO), E_1 (TO), A_1 (LO), A_1 (TO) and E_2 Raman peak positions of hexagonal CdS as well as 1LO, 2LO and TO Raman peak positions of cubic CdS reported in the literature.

Hexagonal CdS						Cubic CdS			
E_1 (LO)	A_1 (LO)	E_1 (TO)	A_1 (TO)	E_2	References	1LO	TO	2LO	References
305	305	235	228	252	[32]	305	246	610	[36]
307	305	243	234	256	[33]	305	—	—	[37]
306.9	303.6	242.6	234.7	255.7	[34]	305	—	604	[38]
308	298	240	228	257	[35]	305	—	—	[39]

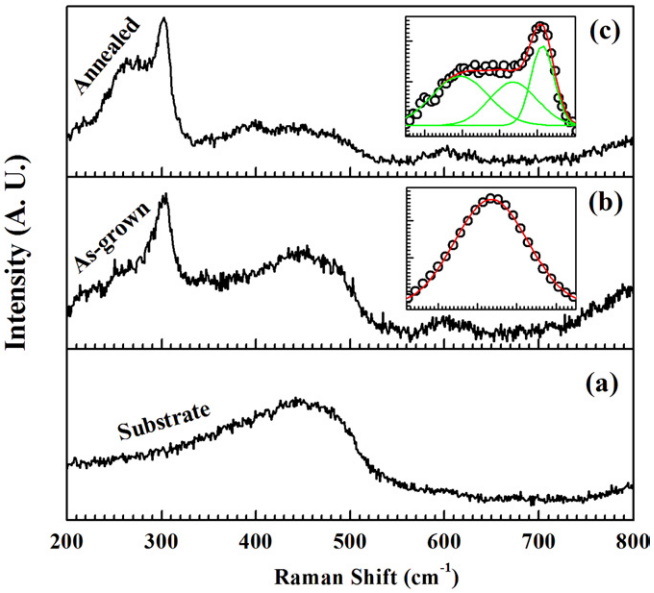

Figure 12. Phase transition of undoped film due to annealing as detected by Raman spectroscopy. (*a*) Substrate, (*b*) as-grown undoped CdS film and (*c*) annealed undoped CdS film.

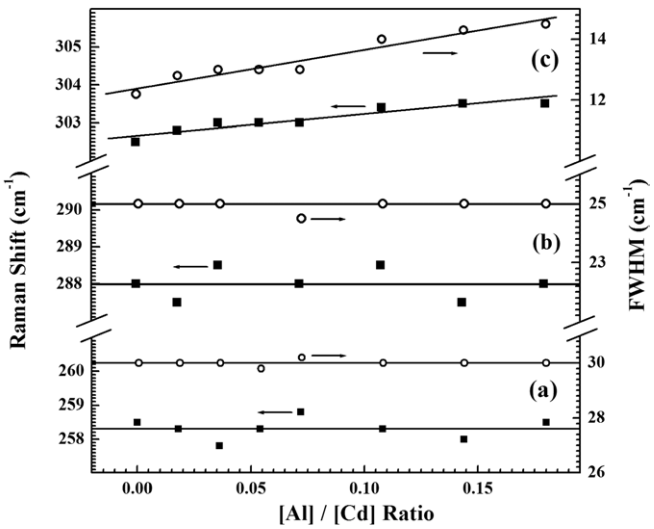

Figure 13. Peak position and FWHM as a function of the [Al]/[Cd] ratio. (*a*) E_2 peak of hexagonal CdS. (*b*) Shifted TO peak of cubic CdS. (*c*) Cubic 1LO or hexagonal A_1(LO)/E_1 (LO) peak.

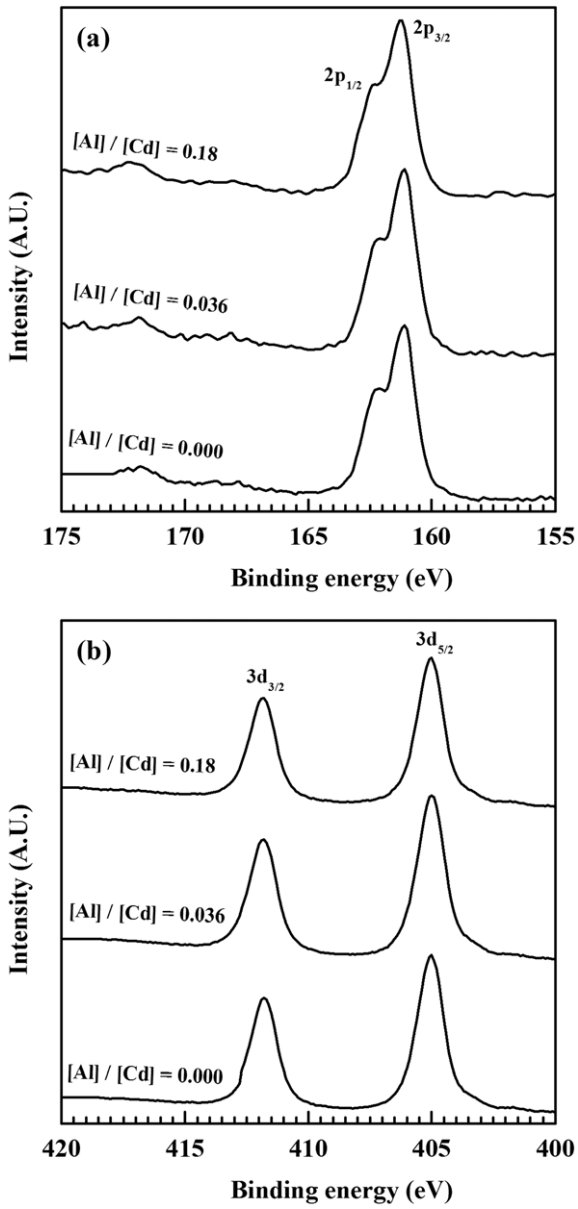

Figure 14. XPS multiplex spectra of the undoped CdS film, Al-doped film grown at [Al]/[Cd] ratios of 0.036 and 0.18. (*a*) S 2p peak. (*b*) Cd 3d peak.

sulfides. No peak shift was detected due to Al doping. Also, no sulfur oxides (166–171 eV) or elemental sulfur (164 eV) [40] are observed. The presence of two peaks arises from a spin–orbit splitting of 1.18 eV between the S $2p_{1/2}$ and the S $2p_{3/2}$ states. Similarly, the binding energy of the Cd $3d_{5/2}$ peak at 405.0 eV (figure 14(*b*)) was found to be the same for all three films. The binding energy of the Cd $3d_{3/2}$ peak was 411.7 eV, which agrees with the 6.74 eV energy splitting between Cd $3d_{5/2}$ and Cd $3d_{3/2}$ states [40]. Both values of binding energy for S 2p and Cd 3d peaks observed in all three films agree well

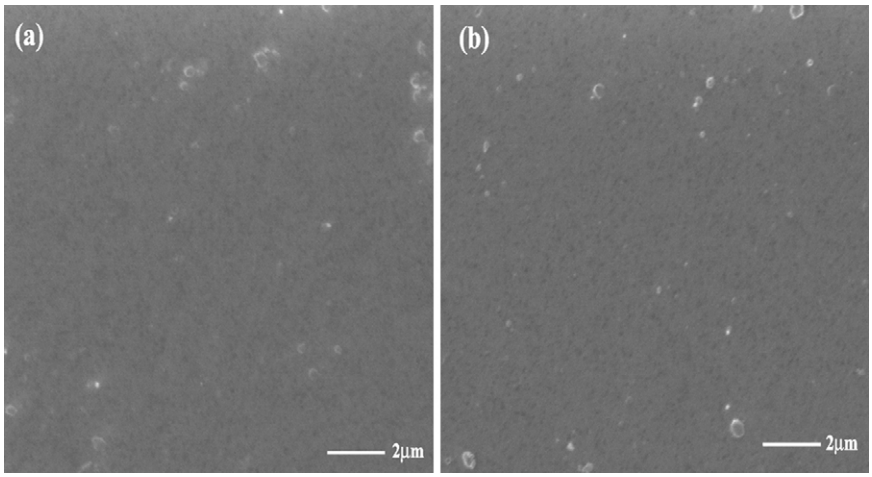

Figure 15. SEM micrographs of (*a*) CdS undoped film and (*b*) Al-doped film grown at a [Al]/[Cd] ratio of 0.036.

with previously reported data on single crystal and thin film CdS [41,42]. It is worth noting that the ratio of S $2p_{3/2}$ signal intensity to that of the Cd $3d_{5/2}$ signal was found to decrease as the [Al]/[Cd] ratio increases. It decreases in the order 0.154, 0.149 and 0.146 as the [Al]/[Cd] ratio increases in the order 0.000 (undoped film), 0.036 and 0.18, respectively. Clearly, Al doping increases the sulfur deficiency in doped films.

SEM images show that Al doping did not affect the morphology of the film. As shown in figure 15, both undoped and Al-doped films are smooth, continuous and uniform with some coverage by scattered crystallite overgrowth that appear to have the same density for both films. These are most probably aggregates due to colloidal particles formed in solution and then adsorbed on the film.

3.2. Investigation of indium doping

Due to the extremely low solubility product of In_2S_3 ($K_{sp} = 10^{-73.24}$) compared with that of CdS ($K_{sp} = 10^{-27.94}$) [43], only two [In]/[Cd] ratios, 0.009 and 0.018, were used. Once $InCl_3$ was added, the solution became turbid and a homogeneous reaction dominated the deposition process. In both cases, the substrate was kept in solution for less than 5 min to avoid deposition of porous, non-adhesive and poor quality layer due to the homogeneous reaction. Although the deposition process was repeated four times using a fresh solution each time, the film obtained in both cases was very thin (about 550 Å). Almost no film was deposited when a higher concentration of indium was used. This is due to the quick depletion of In^{3+} and S^{2-} ions in solution because of the homogeneous reaction that dominated the deposition process from the very beginning. Figure 16 shows transmittance and reflectance spectra of both films. The absorption edge observed for both films is not quite steep as in the case of Al-doped films, which may have to do with the small thickness as well as the inferior quality of both films. According to band gap calculations shown in figure 17, both films appear to have the band gap characteristic of indium sulfide rather than that of CdS. The band gap observed was 2.75 eV and 2.74 eV for films grown at [In]/[Cd] ratios of 0.009 and 0.018, respectively. This

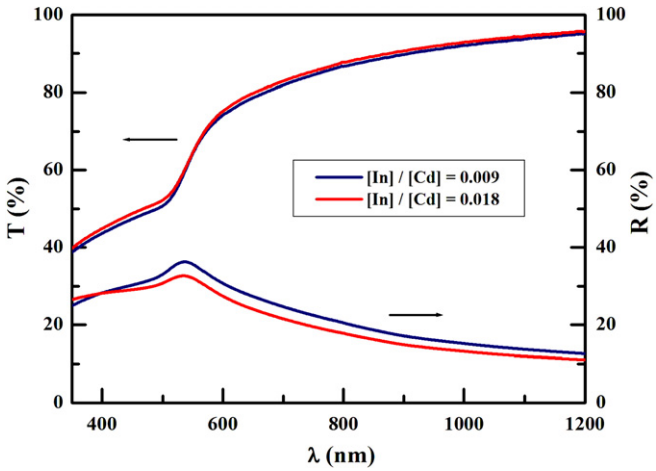

Figure 16. Specular transmittance and reflectance spectra of the films grown at [In]/[Cd] ratios of 0.009 and 0.018.

agrees well with the 2.75 eV bandgap of indium sulfide thin films reported by Lokhande *et al* [44] and Sanz *et al* [45]. As shown in figure 18, the XRD pattern of films grown at the [In]/[Cd] ratio of 0.018 is a mixture of cubic In_2S_3 (JCPDS 032-0456) [46] and Orthorhombic InS (JCPDS 019-0588) [47], with no peaks characteristic of cubic or hexagonal CdS being detected. In general, CBD of indium sulfide or cadmium sulfide takes place when the product of the ion concentration in the solution exceeds the solubility product, K_{sp}. Since K_{sp} of indium sulfide is extremely low compared with that of CdS, the deposition of indium sulfide will dominate and no matter how small the concentration of indium is, it is highly unlikely, if not impossible, to incorporate indium in CdS using CBD. Certainly, our results prove that conclusion.

4. Conclusion

Aluminium *in situ* doping of CdS using CBD proves to be successful. A resistivity as low as 4.6×10^{-2} Ω cm and a carrier density as high as 1.1×10^{19} cm^{-3} were achieved. The bandgap of doped films was found to decrease at first with the Al concentration and then slightly increases and finally saturates

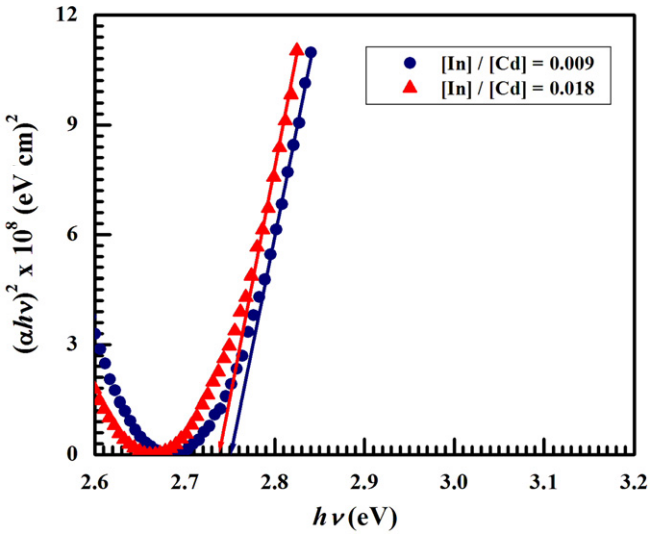

Figure 17. Optical bandgap calculations of films grown at [In]/[Cd] ratios of 0.009 and 0.018.

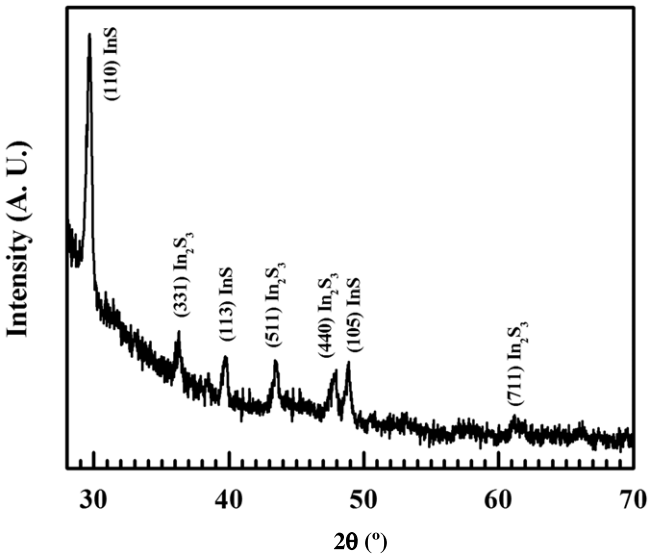

Figure 18. XRD pattern of the film grown at a [In]/[Cd] ratio of 0.018.

at 2.30 eV. The minimum bandgap observed was 2.26 eV at [Al]/[Cd] ratios of 0.018 and 0.036. XRD measurements did not detect any new peaks due to Al doping indicating that incorporation of Al^{3+} ions does not change the crystal structure of the CdS film. It also showed that at a low [Al]/[Cd] ratio, Al^{3+} ions replace Cd^{2+} ions in the lattice substitutionally, and as this ratio increases beyond 0.055, Al^{3+} ions start to enter the lattice both substitutionally and interstitially, until that ratio exceeds 0.11 where most, if not all, Al^{3+} ions incorporated in the lattice occupy interstitial sites. This explains the drop in carrier density and rise in resistivity once the [Al]/[Cd] ratio exceeds 0.055. Micro-Raman measurements show phase transition in all films, due to annealing, where modes of cubic and hexagonal phases were detected. An increase in the FWHM of cubic 1LO or hexagonal A_1(LO)/E_1(LO) peak with the [Al]/[Cd] ratio was observed, which implies an increase in the induced lattice damage as the [Al]/[Cd] ratio increases. XPS spectra showed that, however, Al doping did not cause any shift in the position of the S 2p and Cd 3d peaks; it increased the sulfur deficiency in doped films. SEM images showed that Al doping did not affect the morphology of the CdS film. Finally, we have shown that using CBD, it is highly unlikely, if not impossible, to incorporate indium in CdS. Unlike co-evaporation of CdS and indium [24, 25], CBD is not a suitable technique for growing In-doped CdS films.

Acknowledgments

The authors are grateful to K Scammon of the Advanced Materials Processing and Analysis Center (AMPAC), University of Central Florida, for his help with the XPS measurements. They are also grateful to Professor Aravinda Kar and his group, especially Dr Sachin Bet, of the College of Optics and Photonics, University of Central Florida, for their help with the Hall measurements. This work was partially supported by Apollo Technologies, Inc. and the Florida High Tech Corridor Council.

References

[1] Mokrushin S and Tkachev Y 1961 *Kolloid. Zh.* **23** 438
[2] Kitaev G, Uritskaya A and Mokrushin S 1965 *Russ. J. Phys. Chem.* **39** 1101
[3] Khallaf H, Oladeji I, Chai G and Chow L 2008 *Thin Solid Films* at press (doi:10.1016/j.tsf.2008.01.004)
[4] Khallaf H, Oladeji I and Chow L 2008 *Thin Solid Films* **516** 5967
[5] Dona J and Herrero J 1992 *J. Electrochem. Soc.* **139** 2810
[6] Metin H and Esen R 2003 *Semicond. Sci. Technol.* **18** 647
[7] Rami M, Benamar E, Fahoume M, Chraibi F and Ennaoui A 1999 *Solid State Sci.* **1** 179
[8] Nagao M and Watanabe S 1968 *Japan. J. Appl. Phys.* **7** 684
[9] Nakanishi T and Ito K 1994 *Sol. Energy Mater. Sol. Cells* **35** 171
[10] Guillén C, Martínez M and Herrero J 1998 *Thin Solid Films* **335** 37
[11] Chu T, Chu S, Schultz N, Wang C and Wu C 1992 *J. Electrochem. Soc.* **139** 2443
[12] Nair M, Nair P and Campos J 1988 *Thin Solid Films* **161** 21
[13] Reádigos A, García V, Gomezdaza O, Campos J, Nair M and Nair P 2000 *Semicond. Sci. Technol.* **15** 1022
[14] Sebastian P 1993 *Appl. Phys. Lett.* **62** 2956
[15] Petre D, Pintilie L, Pentia E, Pintilie I and Botila T 1999 *Mater. Sci. Eng.* B **58** 238
[16] Sahu S and Chandra S 1987 *Sol. Cells* **22** 163
[17] Shikalgar A and Pawar S 1979 *Solid State Commun.* **32** 361
[18] Bargale B, Shikalgar A and Pawar S 1979 *Thin Solid Films* **62** 215
[19] Lokhande C and Pawar S 1982 *Solid State Commun.* **44** 1137
[20] Akintunde J 2000 *J. Mater. Sci.: Mater. Electron.* **11** 503
[21] Lee J 2004 *Thin Solid Films* **451–452** 170
[22] Ristova M, Ristov M, Tosev P and Mitreski M 1998 *Thin Solid Films* **315** 301
[23] Ristova M and Ristov M 1998 *Sol. Energy Mater. Sol. Cells* **53** 95
[24] Bertrán E, Morenza J, Esteve J and Codina J 1984 *J. Phys. D: Appl. Phys.* **17** 1679
[25] Hayashi T, Nishikura T, Suzuki T and Ema Y 1988 *J. Appl. Phys.* **64** 3542
[26] Pankove J 1971 *Optical Processes in Semiconductors* (New York: Dover)

[27] Sze S 1981 *Physics of Semiconductor Devices* (New York: Wiley)
[28] Zelaya-Angel O, Alvarado-Gil J, Lozada-Morales R, Vargas H and Ferreira da Silva A 1994 *Appl. Phys. Lett.* **64** 291
[29] Huheey J 1983 *Inorganic Chemistry* 3rd edn (New York: Harper and Row)
[30] Zelaya-Angel O, Castillo-Alvarado F, Avendaño-López J, Escamilla-Esquivel A, Contreras-Puente C, Lozada-Morales R and Torres-Delgado G 1997 *Solid State Commun.* **104** 161
[31] Froment M, Bernard M, Cortes R, Mokili B and Lincot D 1995 *J. Electrochem. Soc.* **142** 2642
[32] Tell B, Damen T and Porto S 1966 *Phys. Rev.* **144** 771
[33] Arguello C, Rousseau D and Porto S 1969 *Phys. Rev.* **181** 1351
[34] Briggs R and Ramdas A 1976 *Phys. Rev.* B **13** 5518
[35] Nusimovici M and Birman J 1967 *Phys. Rev.* **156** 925
[36] Zahn D, Maierhofer C H, Winter A, Reckzügel M, Srama R, Thomas A, Horn K and Richter W 1991 *J. Vac. Sci. Technol.* B **9** 2206
[37] Nagai T, Kanemitsu Y, Yamada Y and Taguchi T 2003 *J. Lumin.* **102–103** 604
[38] Leite R and Porto S 1966 *Phys. Rev. Lett.* **17** 10
[39] Ichimura M, Goto F and Arai E 1999 *J. Appl. Phys.* **85** 7411
[40] Moulder J, Stickle W, Sobol P and Bomben K 1992 *Handbook of X-ray Photoelectron Spectroscopy* ed J Chastain (Minnesota: Perkin-Elmer Corporation)
[41] Rieke P and Bentjen S 1993 *Chem. Mater.* **5** 43
[42] Marychurch M and Morris G 1985 *Surf. Sci.* **154** L251
[43] Sillén L and Martell A 1964 *Stability Constants of Metal–Ion Complexes* (London: Burlington House)
[44] Lokhande C, Ennaoui A, Patil P, Giersig M, Diesner K, Muller M and Tributsch H 1999 *Thin Solid Films* **340** 18
[45] Sanz C, Guillén C and Gutiérrez M 2006 *Thin Solid Films* **511–512** 121
[46] Joint Committee on Powder Diffraction Standards *Powder Diffraction File* No 032-0456
Bonsall S and Hummel F 1978 *J. Solid State Chem.* **25** 379
[47] Joint Committee on Powder Diffraction Standards *Powder Diffraction File* No 019-0588
Duffin W and Hogg J 1966 *Acta Cryst.* **20** 566